



# Observation and Analysis of VLF Nocturnal Multimode Interference Phenomenon based on Waveguide Mode Theory

Sai Yang<sup>1</sup>, You-Tian Niu<sup>1,2,3,4</sup>, Zhe Wang<sup>1</sup>, Xiu-Kun Zhao<sup>1</sup>, Bei Li<sup>1</sup>, Yu-Ling Ding<sup>1</sup>, Ge-Ge Zhao<sup>1</sup>, and An-Qi Zhang<sup>1</sup>

<sup>1</sup>College of Electronic and Electrical Engineering, Henan Normal University, Xinxiang 453007, China; [niuyt22@163.com](mailto:niuyt22@163.com)

<sup>2</sup>Academician Workstation of Electromagnetic Wave Engineering of Henan Province, Xinxiang 453007, China

<sup>3</sup>Key Laboratory of Optoelectronic Sensing Integrated Application of Henan Province, Xinxiang 453007, China

<sup>4</sup>Engineering Laboratory of Intelligent Additive Manufacturing of Henan Province, Xinxiang 453007, China

Received 2023 July 24; revised 2023 October 3; accepted 2023 October 23; published 2023 December 12

## Abstract

Very low frequency (VLF) signals are propagated between the ground-ionosphere. Multimode interference will cause the phase to show oscillatory changes with distance while propagating at night, leading to abnormalities in the received VLF signal. This study uses the VLF signal received in Qingdao City, Shandong Province, from the Russian Alpha navigation system to explore the multimode interference problem of VLF signal propagation. The characteristics of the effect of multimode interference phenomena on the phase are analyzed according to the variation of the phase of the VLF signal. However, the phase of VLF signals will also be affected by the X-ray and energetic particles that are released during the eruption of solar flares, therefore the two phenomena are studied in this work. It is concluded that the X-ray will not affect the phase of VLF signals at night, but the energetic particles will affect the phase change, and the influence of energetic particles should be excluded in the study of multimode interference phenomena. Using VLF signals for navigation positioning in degraded or unavailable GPS conditions is of great practical significance for VLF navigation systems as it can avoid the influence of multimode interference and improve positioning accuracy.

*Key words:* waves – methods: data analysis – Sun: flares – Sun: X-rays – gamma-rays

## 1. Introduction

The Global Positioning System (GPS) offers crucial positioning capabilities to military, civilian, and commercial users worldwide. In numerous complex environments, GPS access is restricted or signals can be lost. GPS is especially susceptible to interference during solar storms. Establishing radio navigation based on very low frequency (VLF) radio signals focuses on the possibility of positioning, navigating, and timing using VLF signals in GPS-degraded or unavailable conditions (Curro et al. 2018). VLF radio frequency range 3–30 kHz is widely utilized for navigation, timing (Niu et al. 2009) earthquake prediction (Singh et al. 2005), submarine communication (Shi et al. 2011), mineral resources detection (Niu et al. 2016), and space environment monitoring (Su et al. 2019) because of its long wavelength, low losses, stable amplitude and phase, and strong permeability.

VLF waves propagate through the ground-ionosphere waveguide, and in ideal single-mode propagation, the daily variation curve of VLF phase takes on a consistent trapezoidal shape. When the entire propagation path is entirely during day or night, the phase stabilizes at the respective fixed values, with the daytime phase overtaking the nighttime phase. When the diurnal boundary intersects the propagation path, resulting in a diurnal transition, the propagation phase undergoes a drift and

shifts along two oblique lines. But in fact, in the transition period between sunrise and sunset, due to the existence of mode-conversion interference, the propagation phase curve is not monotonically smooth, but appears “step” shaped changes, and sometimes even the whole cycle of “phase slip” phenomenon (Wang 2006).

According to the distance, the propagation area of VLF signals can be divided into near-field, far-field, and waveguide regions (Niu et al. 2021). In the waveguide region, where multiple waveguide modes of various orders coexist, the superposition of waveguide modes of each order results in the total electromagnetic field’s amplitude and phase changes in an oscillatory form with distance, which is known as multimode interference. In the ground-ionospheric waveguide for VLF, numerous lower-order waveguide modes can typically be excited simultaneously. Each of these modes propagates in the waveguide with a variable excitation power, decay rate, and phase velocity, with the decay rate rising with mode order. In the distance from the transmitting antenna within a few thousand kilometers of the middle and close distances, since the higher-order mode has a sufficiently strong amplitude compared to the first-order mode with the lowest attenuation, in this way, the field strength and phase of the wave do not vary monotonically with the distance, but take the form of

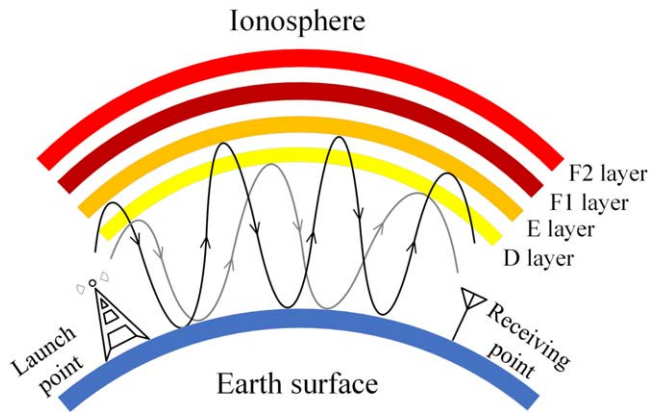


**Figure 1.** Schematic diagram of ground ionospheric waveguide.

oscillations, and this region is called the multimode interference region. Due to the extreme attenuation of their effects at a sufficient distance, the higher order modes are insignificant. The interference phenomenon vanishes at this stage, leaving only the first-order modes with little decay; this region is known as the single-mode region. In general, the interference is more significant at night than during the day, and higher frequency waves are more significant than lower frequency waves (Pan 2004). There are moments when the signal is much weaker at specific points in the interference zone and the phase stability of the received signal is significantly worsened. This will negatively impact VLF radio communication, navigation, timing, and frequency comparison.

Numerous local and foreign academics have researched and spoken about the properties and impacts of multi-modal interference phenomena. Crombie (1964) used the concept of mode conversion to explain the phase step and amplitude decay at dawn and dusk. Wang (2006) discovered that the periodic slip of the VLF propagation phase is a peculiar multimode interference phenomenon that occurs during the transition between sunrise and sunset. Chand & Kumar (2017) investigated the VLF modal interference distance and nighttime VLF reflection height for east–west propagation paths using amplitude minima at sunrise and sunset. He et al. (2018) analyzed the multimode interference and phase standard deviation of VLF wave propagation in anisotropic ground ionospheric waveguides. Xin (2019) studied the propagating decay of the first fourth order mode at very low frequencies. In contrast, this article studies the characteristics of the phenomenon of close range multimode interference at night, which is different in terms of research period and research distance. By receiving VLF signals at 11.9, 12.6 and 14.9 kHz from the East Sub-station of the Alpha Navigation System at Qingdao Station, we analyzed the phase changes and observed and studied the VLF multimode interference.

## 2. Propagation and Observation System

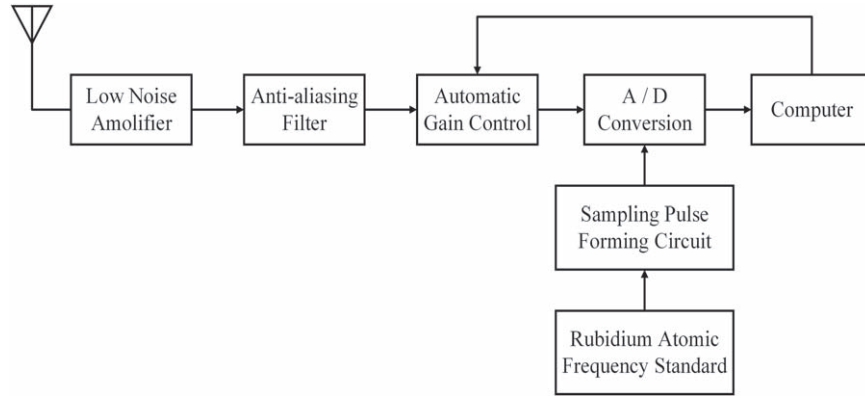
### 2.1. Principle of Very Low Frequency Propagation

The ground ionospheric waveguide, which is formed between the bottom border of the low ionosphere and the Earth’s surface, is where VLF primarily propagates, usually analyzed using the concept of “waveguide mode.” The propagation pattern is shown in Figure 1. The ionosphere is usually divided into three regions from low to high, the D, E, and F layers. The D layer, which is located about 70 km from the Earth’s surface, absorbs a lot of short-wave radio waves and has a lot of electrons during the day. At night, it essentially disappears; the electron density of the E layer is roughly 90 km from the Earth’s surface, the electron density has diurnal and seasonal variations. It is also significantly lower at night than it is during the day, and it climbs in height; about 130 km separates the F layer from the Earth’s surface. The F layer, which is present both day and night and is split into F1 and F2 layers during the day and combines into one layer at night, contains irregular abnormalities. The upper wall of the ground-ionosphere waveguide is the ionosphere D layer during the day, the D layer disappears at night, and the reflected upper wall is the E layer (Devi et al. 2008). When the VLF signal propagates in the waveguide space between the transmitting station and the receiving station, it is refracted many times in the ground-ionosphere waveguide and propagates forward in the waveguide cavity (Zhao et al. 2023).

### 2.2. Transmitting and Receiving Systems

The VLF signal transmission station in this paper consists mainly of the East Sub-station in Khabarovsk, the Main Station in Novosibirsk, and the West Sub-station in Krasnodar in the Russian Alpha navigation system (Huang & Ji 2005), with the receiving station located in Qingdao, Shandong province. This article mainly analyzes the VLF signal under the propagation path from the Alpha navigation system to Qingdao, and Table 1 provides basic information about the VLF transmitting and receiving stations.

The block diagram of the VLF signal receiving system is shown in Figure 2. The system is developed with software radio technology and has good reliability. It is mainly composed of four parts: receiving antenna, digital VLF software radio receiver, rubidium atomic frequency scale, and computer (Niu et al. 2009, 2014b; Niu & Bi 2016). The VLF signal received by the antenna is sampled after passing through the low noise amplifier, anti-aliasing filter and automatic gain control. The standard sampling interval of the sampling pulse circuit used is provided by the rubidium atomic frequency standard. After sampling, conduct A/D conversion and input to the computer. The computer will feed back to the automatic gain control link according to the received signal, and


**Figure 2.** VLF Signal Receiving System.

**Table 1**

Basic Information of Alpha Navigation System Transmitting Station and Qingdao Receiving

Transmitting/Receiving Station	Latitude and Longitude	VLF Frequency (kHz)
Khabarovsk (East Sub-station)	50°04'N 136°36'E	11.9, 12.6, 14.9
Novosibirsk (Main Station)	55°45'N 84°26'E	11.9, 12.6, 14.9
Krasnodar (West Sub-station)	45°24'N 38°09'E	11.9, 12.6, 14.9
Qingdao City (Receiving Station)	36°07'N 120°42'E	11.9, 12.6, 14.9

accurately regulate the signal to ensure its accuracy. The phase measurement accuracy of this system is  $\pm 1 \mu\text{s}$ .

Figure 3 shows the propagation path of the Alpha VLF navigation system to Qingdao. Qingdao Station is located in Qingdao City, Shandong Province, whose geographical coordinates are (36°07'N, 120°42' E) (Niu et al. 2015). It receives VLF signals at three operating frequencies of 11.9, 12.6, and 14.9 kHz from the East Sub-station (HAB), Main Station (NOV), and West Sub-station (KRA) of the Alpha Very Low Frequency Navigation System. The digital VLF software radio receiver designed through Figure 2 records and monitors data every 3 minutes and receives VLF signals throughout the day.

### 3. Analysis Method and Observation Results

#### 3.1. Theory and Data Analysis

The VLF signal is transmitted in ground and low ionospheric waveguides and is analyzed using the waveguide mode theory. In the transmission process of the VLF signal, the phenomenon

of multimode propagation exists because the transmitting antenna will excite multi-order wave mode in a relatively close distance from the transmitting platform. However, with the increase of the propagation distance, the higher-order wave mode attenuates greatly (Niu et al. 2017).

According to the waveguide mode theory (Wait 1959; Liu 1987), for the  $n$ th order mode, the phase propagation velocity  $v_p$  of the VLF signal has the following expression:

$$v_p = v_c \left[ 1 - \lambda^2 \left( \frac{n - \frac{1}{2}}{2h_0} \right)^2 \right]^{-\frac{1}{2}} \left( 1 - \frac{h_0}{2a} \right) \quad (1)$$

For the first-order mode, substituting  $n = 1$  into Equation (1) yields the expression for the propagation phase velocity  $v_p$  of the VLF signal as:

$$v_p = v_c \left( 1 - \frac{\lambda^2}{16h_0^2} \right)^{-\frac{1}{2}} \left( 1 - \frac{h_0}{2a} \right) \quad (2)$$

If the ionospheric equivalent reflection height varies as  $\Delta h$  and the corresponding VLF signal phase varies as  $\Delta\varphi$ , the relation is:

$$\Delta\varphi = -2\pi d \times \left( \frac{h_0}{2a} + \frac{\lambda^2}{16h_0^2} \right) \frac{\Delta h}{\lambda h_0} \quad (3)$$

The relation between the ionospheric equivalent reflection height variation  $\Delta h$  and the VLF signal phase variation  $\Delta\varphi$  can be obtained as follows:

$$\Delta h = \frac{\lambda h_0 \Delta\varphi}{2\pi d \left( \frac{h_0}{2a} + \frac{\lambda^2}{16h_0^2} \right)} \quad (4)$$

where  $n$  represents the order of the propagation mode;  $v_c$  is the speed of propagation of light in space, which is about  $2.998 \times 10^8 \text{ m} \cdot \text{s}^{-1}$ ;  $\lambda = \frac{v_c}{f}$  denotes the wavelength of the VLF signal, where  $f$  is the frequency of the VLF signal, which is 11.9, 12.6, and 14.9 kHz;  $h_0$  indicates the equivalent



Figure 3. VLF Signal Observation System.

reflectance height of the ground ionosphere. At mid-latitudes,  $h_0$  is about 70 km during the day and 87 km at night in summer, with the height rising somewhat in winter to about 72 km during the day and 87 km at night (Pan 2004);  $a$  is the mean radius of the Earth, which is about 6371.4 km, and  $d$  is the distance of the great circle path between the transmitting and receiving points.

Due to the different observation paths in Qingdao, the equation of the relation between the peak flux density of X-rays and the variation  $h$  of the ionospheric equivalent reflection height is refitted in this paper (Niu et al. 2014c). Based on the 90 flare phase anomalies observed by VLF receiver from 08:00 to 16:00 in 2000 and 2001, the least squares method is used to fit the East Sub-station to Qingdao route, and the fitting equation is:

$$F_0 = 2.235e^{0.1638|\Delta h|} \times 10^{-3} \quad (5)$$

By observing a large amount of solar flare data and using GOES satellite data as a standard, the flare level can be calculated using the VLF method, thereby analyzing the impact of solar flares on the propagation of VLF signals. According to the different propagation distances, when the propagation distance is close, formula (1) can be used to calculate the multi mode phase velocity of VLF during the propagation process. When the propagation distance is far, formula (2) can be used to obtain the propagation phase velocity of the first mode. Then, combining formulas (3) and (4), the equivalent reflection height change value of the ionospheric D-layer and the abnormal change of VLF signal phase can be calculated when a solar flare erupts. Finally, according to the fitting formula (5) under the propagation path from East Satellite Station to

Table 2  
Solar Flare Level

$F/(\text{erg}/(\text{cm}^2 \cdot \text{s}))$	Flare Level
$F < 10^{-4}$	A
$10^{-4} \leq F < 10^{-3}$	B
$10^{-3} \leq F < 10^{-2}$	C
$10^{-2} \leq F < 10^{-1}$	M
$F \geq 10^{-1}$	X

Qingdao, the peak X-ray flux density of the solar flare can be calculated, and then the flare level can be calculated.

### 3.2. Observation Result

With the onset of solar flares, a significant amount of energetic charged particles emitted by the Sun will reach the Earth in 1–3 days in addition to X-rays reaching the Earth in approximately 8.3 minutes and impacting the environment for satellite navigation and communication. The phase change of VLF is very sensitive to the SID (Sudden Ionic Disturbance) caused by X-rays (Selvakumaran et al. 2015) and energetic particles (Peter et al. 2006), etc. emitted during solar activity. When influenced by X-rays and energetic particles, the phase of VLF signals will undergo abnormal changes. According to the magnitude of X-ray flux, the flare level can be divided into five levels (Niu et al. 2014a), as shown in Table 2. Each level in A, B, C, and M is divided into levels 1 to 9 based on strength, while level X has no upper limit.

The great circle path distance from Qingdao to the East Sub-station is 2029.6 km, the great circle path distance to the Main Station is 3481.5 km, and the great circle path distance to the

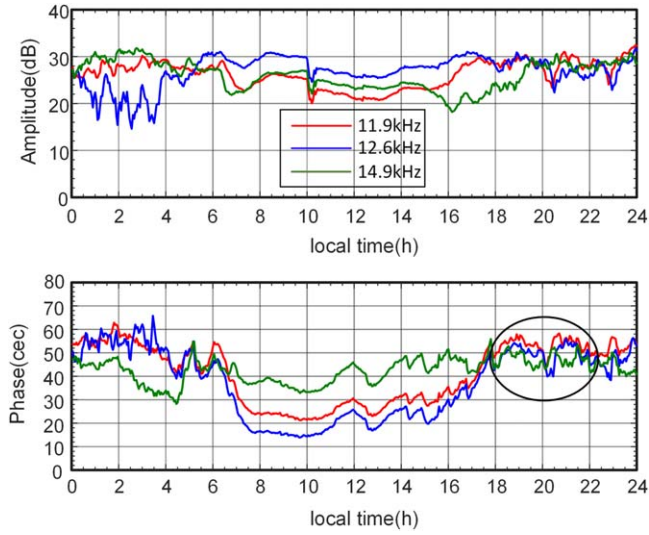


**Figure 4.** Amplitude and phase change curve of VLF signal from East Sub-station to Qingdao on 2000 January 10.

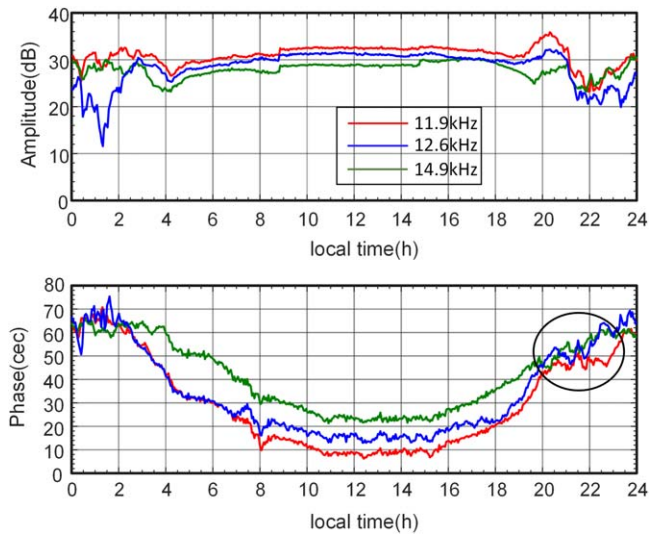


**Figure 5.** Amplitude and phase change curve of VLF signal from East Sub-station to Qingdao on 2000 July 22.

West Sub-station is 6720.0 km, according to the formula for calculating the great circle distance of the Earth (Fu 1990). As this article focuses on the phenomenon of multimode interference in VLF at night at medium to close distances, the X-rays generated during solar flares do not affect the phase of VLF signals at night, while the energetic particles generated will have an impact. In order to prevent the results of the analysis from being impacted, energetic particles interference must be excluded while analyzing the effect of multimode interference on the phase of VLF signals.

**Table 3**

Solar Flare Data Monitored by GOES Satellite from 2000 January 7–9 and 2000 July 19–21

Date	Start	Max	End	NOAA/USAF	
				X-ray Flare Level	Flux
2000-01-7	06:16	06:23	06:32	C1.6	$1.3 \times 10^{-3}$
2000-01-7	19:22	19:28	19:33	C3.2	$1.4 \times 10^{-3}$
2000-01-8	01:18	01:40	01:51	C5.6	$6.8 \times 10^{-3}$
2000-01-8	02:36	02:59	03:07	C2.9	$4.3 \times 10^{-3}$
2000-01-9	00:08	00:45	01:16	C6.0	$1.5 \times 10^{-2}$
2000-01-9	16:15	16:27	16:51	C3.2	$5.5 \times 10^{-3}$
2000-07-19	03:34	03:45	04:14	M3.3	$6.7 \times 10^{-2}$
2000-07-19	14:45	15:26	15:50	M6.4	$1.6 \times 10^{-1}$
2000-07-20	17:21	18:06	18:39	M3.6	$1.1 \times 10^{-1}$
2000-07-20	21:16	21:23	21:33	C7.0	$6.1 \times 10^{-3}$
2000-07-21	04:22	04:25	04:28	M5.0	$1.0 \times 10^{-2}$
2000-07-21	22:30	22:37	22:43	M5.5	$2.5 \times 10^{-2}$

### 3.2.1. The Influence of Energetic Particles

Figures 4 and 5 show the amplitude and phase curves of the VLF signal transmitted by the Alpha Navigation System East Sub-station in Qingdao on 2000 January 10 and 2000 July 22. It can be seen from the figures that there were abnormal changes in the VLF signal phase from 18:00 to 22:00 on 2000 January 10 (black circle in Figure 4) and from 20:00 to 23:00 on 2000 July 22 (black circle in Figure 5). The propagation area from Qingdao to East Sub-station belongs to the waveguide region and may be affected by multimode interference and energetic particles.

Table 3 shows the solar flare data from 2000 January 7–9 to 2000 July 19–21. Due to the large amount of data, only two sets of data with larger flare levels are listed for analysis every day. Here, Start is the time when solar flare starts to erupt, Max is the peak time, and End is the end time. X-ray flare level is the level of solar flare corresponding to the X-ray emitted during the eruption of solar flare, and Flux is the flux released during the eruption of the flare, in unit  $\text{W} \cdot \text{m}^{-2}$ . Due to the fact that energetic particles generated during solar flares only reach Earth after 1–3 days, solar flares that occurred on 2000 January 7–9 and 2000 July 19–21 may have an impact on the phase of VLF signals on 2000 January 10 and 2000 July 22.

Figure 6 shows the energetic particles flow maps of GOES satellite on 2000 January 10 and 2000 July 22. It can be seen from the figures that the density of energetic particles began to significantly increase at 03:00 on 2000 January 10 and 20:00 on 2000 July 22. It can be inferred that the oscillation of the VLF signal phase observed in this observation was caused by energetic particles generated by the solar flare eruption.

### 3.2.2. The Influence of Multimode Interference

The amplitude and phase curves of the VLF signals received in Qingdao on 2001 November 13, and 2002 February 25, are

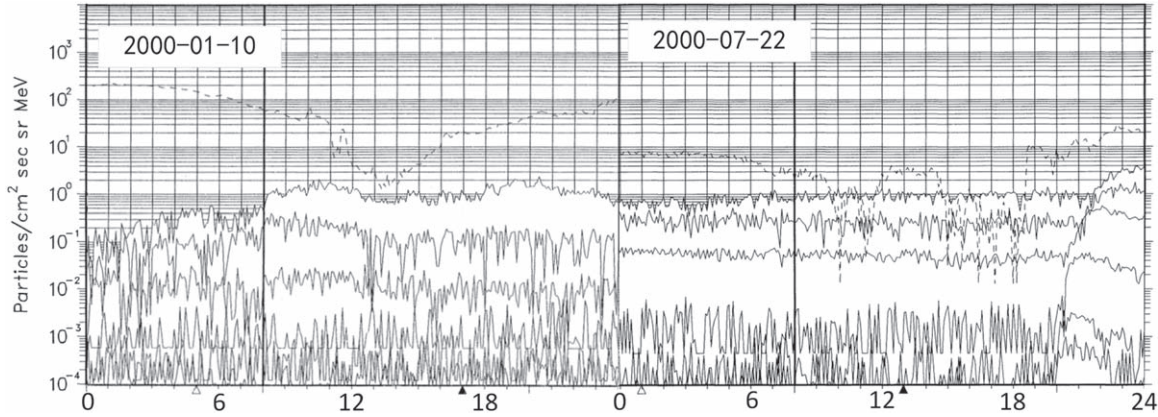


Figure 6. Energetic particles flow chart of GOES satellite on 2000 January 10 and 2000 July 22.

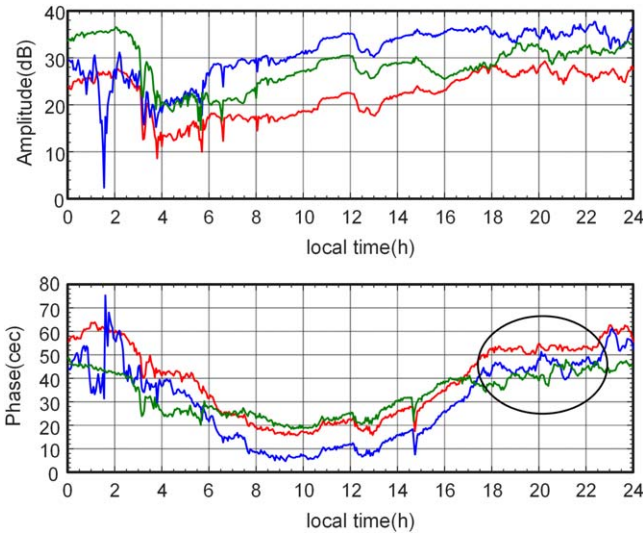


Figure 7. Amplitude and phase change curve of VLF signal from East Sub-station to Qingdao on 2001 November 13.

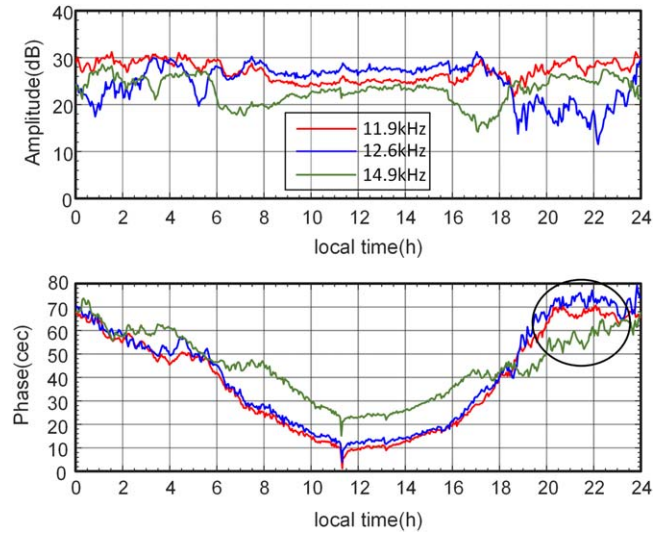


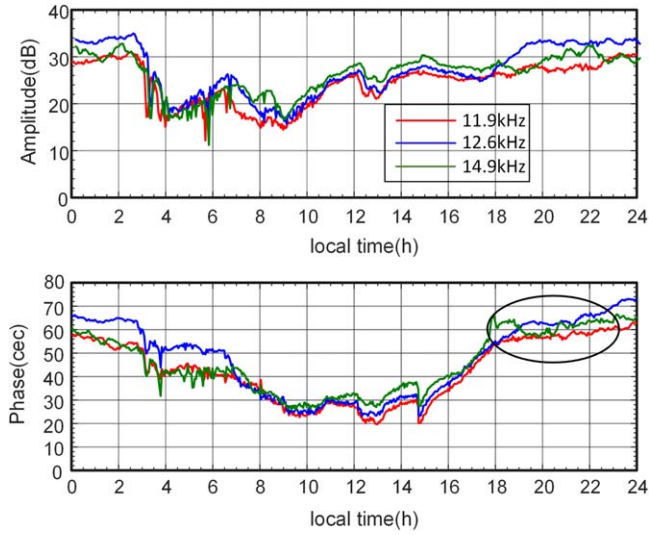
Figure 8. Amplitude and phase change curve of VLF signal from East Sub-station to Qingdao on 2002 February 25.

shown in Figures 7–12. Data from the East Sub-station to Qingdao are shown in Figures 7 and 8, data from the Main Station to Qingdao are shown in Figures 9 and 10, and data from the West Sub-station to Qingdao are shown in Figures 11 and 12. From Figures 7 and 8, it can be seen that there was an abnormal phase change in the VLF signal from 18:00 to 22:45 on 2001 November 13 (black circle in Figure 7) and from 20:00 to 23:00 on 2002 February 25 (black circle in Figure 8). The black circles in Figures 9 and 10 are relatively less oscillatory, while the black circles in Figures 11 and 12 are closer to a regular VLF signal phase diurnal variation curve. This indicates that as the distance increases, the influence of multimode interference on VLF signals decreases. When the range exceeds the multimode region, the propagation of VLF

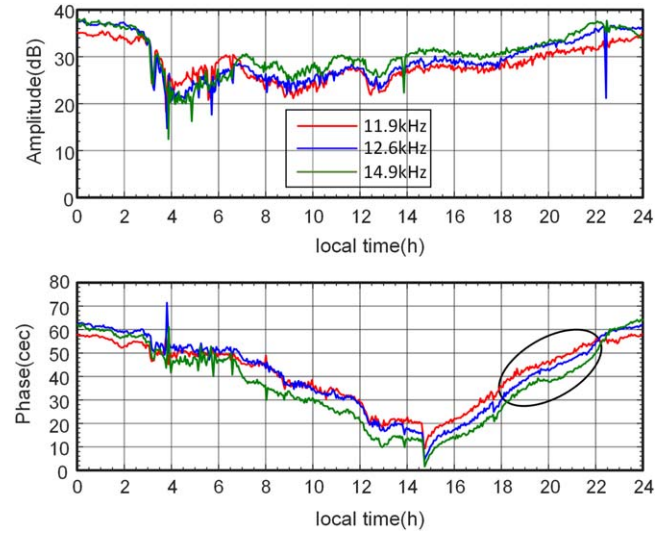
signals is mainly the first-order mode and will no longer be affected by multimode interference.

Table 4 shows the solar flare data from 2001 November 10–12 and 2002 February 22–24. Similarly, only two sets of data with larger flare levels are listed daily for analysis. The energetic particles in these days may have an impact on the phase change of the VLF signal on 2001 November 13 and 2002 February 25.

Figure 13 shows the energetic particles flow charts of the GOES satellite on 2001 November 13 and 2002 February 25. It can be seen from the charts that the energetic particles flow shows a relatively stable state during these two days. In summary, it can be inferred that the phase anomaly changes that occurred from 18:00 to 22:45 on 2001 November 13 and from 20:00 to 23:00 on 2002 February 25 are not related to the



**Figure 9.** Amplitude and phase change curve of VLF signal from Main Station to Qingdao on 2001 November 13.



**Figure 11.** Amplitude and phase change curve of VLF signal from West Substation to Qingdao on 2001 November 13.

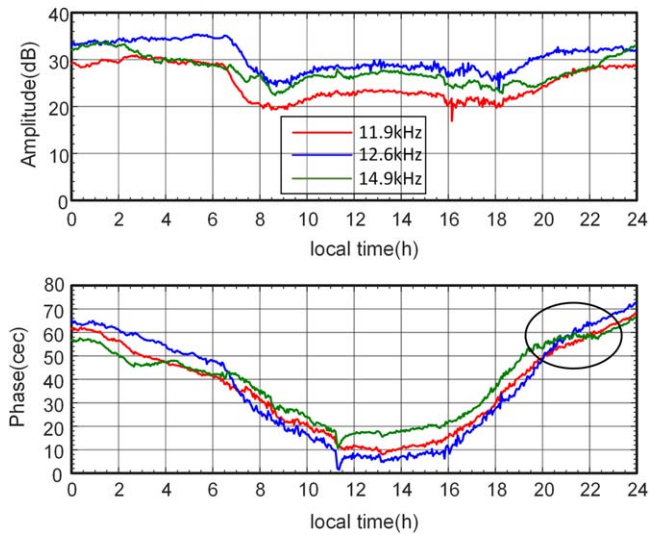


**Figure 10.** Amplitude and phase change curve of VLF signal from Main Station to Qingdao on 2002 February 25.

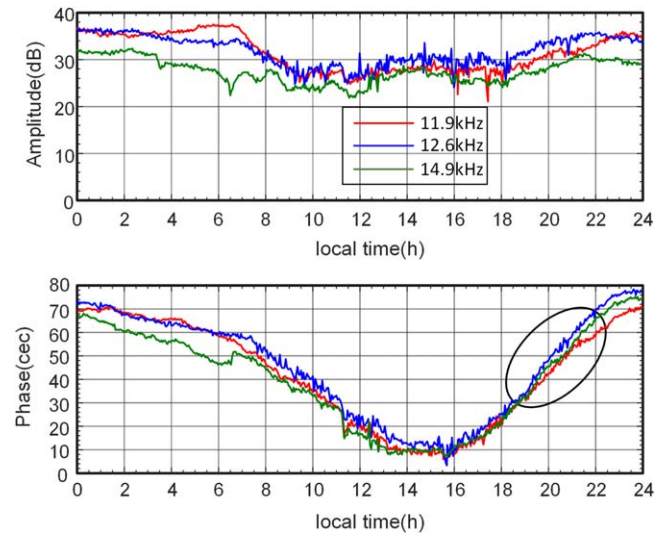


**Figure 12.** Amplitude and phase change curve of VLF signal from West Substation to Qingdao on 2002 February 25.

energetic particles generated during the solar flare eruption. Furthermore, it can be inferred that these moments are influenced by multimode interference phenomena.

### 3.2.3. The Influence of X-Rays

As this article focuses on the impact of multimode interference on the phase of VLF signals at night, the X-ray emitted by solar flares does not affect the phase at night, but can have an impact during the day. From Figures 7 and 8, it can be seen that the phase of the VLF signal showed significant

leading phenomena at 14:30–15:00 on 2001 November 13 and 11:00–11:30 on 2002 February 25. Therefore, the phase anomaly was analyzed. Table 5 shows the solar flare data received by the VLF signal receiving system from the Alpha East Sub-station to Qingdao path, where Start, Max, and End have the same meanings as in the previous table,  $\Delta\varphi_1$ ,  $\Delta\varphi_2$  and  $\Delta\varphi_3$  are the phase change caused by a sudden phase anomaly in the VLF signal, expressed in percentage cycles (cec, 1 cec =  $3^\circ.6$ ) (Wang et al. 2022). Table 6 shows the solar flare data monitored by GOES satellite.

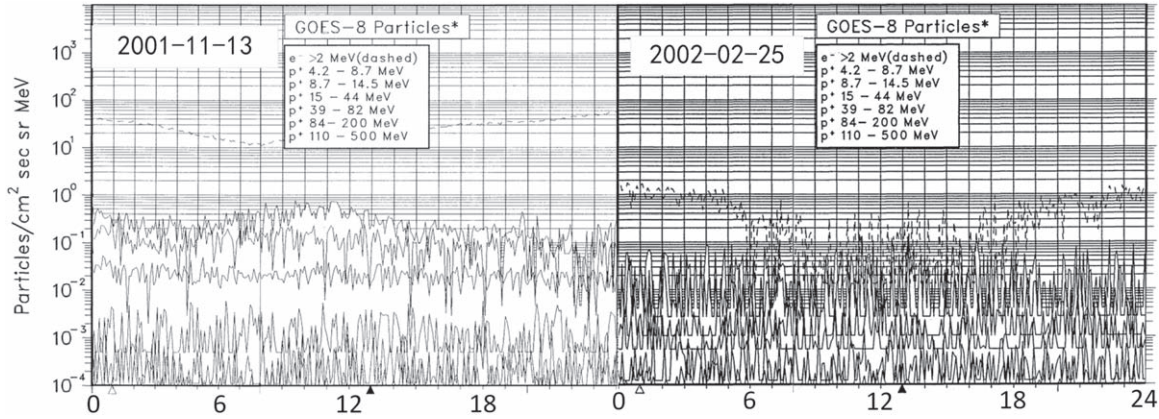


Figure 13. Energetic particles flow chart of GOES satellite on 2001 November 13 and 2002 February 25.

Table 4  
Solar Flare Data Monitored by GOES Satellite from 2001 November 10–12 and 2002 February 22–24

Date	Start	Max	End	NOAA/USAF	
				X-ray Flare Level	Flux
2001-11-10	02:23	02:41	03:24	M1.9	$4.7 \times 10^{-2}$
2000-11-10	08:42	08:50	08:58	M1.0	$7.1 \times 10^{-3}$
2001-11-11	03:47	04:00	04:09	M2.3	$1.8 \times 10^{-2}$
2001-11-11	18:54	19:03	19:07	M1.4	$5.8 \times 10^{-3}$
2001-11-12	15:52	15:57	16:01	M1.6	$5.2 \times 10^{-3}$
2001-11-12	16:33	17:38	18:09	C7.0	$2.5 \times 10^{-2}$
2002-02-22	04:27	04:32	04:50	M1.5	$8.2 \times 10^{-3}$
2002-02-22	07:56	08:07	08:22	M4.4	$2.7 \times 10^{-2}$
2002-02-23	07:08	07:40	08:16	C4.8	$4.7 \times 10^{-3}$
2002-02-23	14:12	14:35	14:51	C2.9	$1.5 \times 10^{-3}$
2002-02-24	06:41	06:50	07:03	C5.2	$4.9 \times 10^{-3}$
2002-02-24	22:48	22:57	23:32	C4.4	$3.5 \times 10^{-3}$

Table 5  
Solar Flare Data Received by the VLF Signal Receiving System Under the Alpha East Sub-station to Qingdao Path on 2001 November 13 and 2002 February 25

Date	Start	Max	End	Outlier of VLF Signal of East Sub-station			Calculation of Flare Level
				$\Delta\varphi_1$ (cec)	$\Delta\varphi_2$ (cec)	$\Delta\varphi_3$ (cec)	
2001-11-13	14:36	14:40	14:45	10.92	10.88	10.91	M1.5
2002-02-25	11:12	11:15	11:22	7.48	7.46	7.49	C8.2

The results derived using the flare calculation technique in the previous section were determined to be essentially consistent with the flare data given by the GOES satellite through the comparison of Tables 5 and 6. At 14:36 on 2001 November 13 and at 11:12 on 2002 February 25, solar flares are therefore considered to have occurred. As a result, it can be inferred that the phase anomalies in these two locations are caused by X-rays generated by solar flare eruptions.

Table 6  
Solar Flare Data Monitored by GOES Satellite on 2001 November 13 and 2002 February 25

Date	Start	Max	End	NOAA/USAF	
				X-ray Flare Level	Flux
2001-11-13	14:36	14:40	14:45	M1.5	$2.6 \times 10^{-3}$
2002-02-25	11:12	11:15	11:22	C8.1	$2.3 \times 10^{-3}$

#### 4. Conclusion

In situations where GPS navigation is not available, VLF can be used for navigation and positioning. This article analyzes and discusses the VLF signals received in Qingdao from the Alpha navigation system, and investigates the impact of multimode interference on VLF signals, leading to the following conclusions:

- (1) From the data received in Qingdao from the East Substation, it can be observed that the phase of the three frequencies is affected to varying degrees in the multimode interference region. The frequency of 14.9 kHz is more significantly affected compared to 11.9 and 12.6 kHz. However, on 2002 February 25, the frequencies of 11.9 and 12.6 kHz were hardly affected by multimode interference, while 14.9 kHz experienced noticeable interference. This confirms that higher-frequency waves are more significantly affected by multimode interference compared to lower-frequency waves.
- (2) When the phase of the VLF signal undergoes abnormal changes, it may be due to X-rays and energetic particles generated by solar flare eruptions and the influence of multimode interference. The X-rays emitted by solar flares will have a phase impact on the VLF signal during the day and will not have an impact at night, while energetic particles will have an impact on the phase of the VLF signal during both day and night. When studying the impact of multimode interference on nighttime VLF signals, it is necessary to exclude the interference of energetic particles to avoid affecting the research results.

This study adopts a combined approach of theoretical analysis and observational data to investigate the impact of multimode interference on the amplitude and phase of VLF signals. It carries significant practical implications for VLF wireless communication, navigation, and positioning systems. However, since this study focuses on the multimode interference phenomenon of VLF signals at medium-range distances, the applicability of this research method to closer-range paths is yet to be determined. It requires further analysis

and discussion of the multimode interference phenomenon on different paths and distances in order to enhance the understanding of its impact on VLF signals.

#### Acknowledgments

This research was supported by the National Natural Science Foundation of China (U1704134). The Solar-Terrestrial environment plots and X-ray flux used in this paper are from the website of the National Oceanic and Atmospheric Administration (NOAA): <https://satdat.ngdc.noaa.gov/sem/goes/data/full/>.

#### References

- Chand, A. E., & Kumar, S. 2017, *RaSc*, **52**, 1004  
 Crombie, D. D. 1964, *J. Res. Natl. Bur. Stand., Sect. D*, **68**, 27  
 Curro, J., Raquet, J., & Borghetti, B. 2018, *Navigation*, **65**, 549  
 Devi, M. I., Khan, I., & Madhusudhana Rao, D. N. 2008, *EP&S*, **60**, 737  
 Fu, Z.-Z. 1990, *J. Civ. Aviat. Inst. China*, **8**, 1  
 He, T., Zheng, J., Pan, W. Y., & Li, K. 2018, *ITAP*, **66**, 7265  
 Huang, J., & Ji, C. S. 2005, *Dao Hang*, **41**, 10  
 Liu, W. T. 1987, *ChJSS*, **7**, 185  
 Niu, Y. T., & Bi, Y. X. 2016, *J. Henan Normal Univ. (Nat. Sci. Ed)*, **44**, 70  
 Niu, Y. T., Bi, Y. X., Li, L., & Li, D. D. 2016, *PrGeo*, **31**, 280  
 Niu, Y. T., Chen, J. F., Hao, H. Z., Wang, H. B., & Zhang, Z. Y. 2009, *J. Henan Normal Univ. (Nat. Sci. Ed)*, **37**, 64  
 Niu, Y. T., Li, D. D., Li, L., & Wei, S. J. B. Y. X. 2015, *J. Henan Normal Univ. (Nat. Sci. Ed)*, **43**, 34  
 Niu, Y. T., Li, L., Zhao, X. Z., et al. 2014a, *PrGeo*, **29**, 2526  
 Niu, Y. T., Li, L., Zhao, X. Z., et al. 2014b, *Sci. Technol. Eng.*, **14**, 203  
 Niu, Y. T., Piao, J. L., Su, Y. F., & Zhang, Y. M. 2017, *J. Henan Normal Univ. (Nat. Sci. Ed)*, **45**, 31  
 Niu, Y. T., Wang, L., Li, W. Q., et al. 2021, *Insul. Surge Arresters*, **9**  
 Niu, Y. T., Zhang, Y. X., Xie, Y. T., Li, D. D., & Li, L. 2014c, *PrGeo*, **29**, 1426  
 Pan, W. Y. 2004, National Defence Industry Press  
 Peter, W. B., Chevalier, M. W., & Inan, U. S. 2006, *JGRA*, **111**, A03301  
 Selvakumaran, R., Maurya, A. K., Gokani, S. A., et al. 2015, *JASTP*, **123**, 102  
 Shi, W., Ye, X. F., & Hu, D. M. 2011, *Digital Technol. Appl.*, **7**, 2  
 Singh, B., Kushwah, V., Singh, V., & Tomar, M. M. H. 2005, *IJRSP*, **34**, 221  
 Su, Y. F., Dong, L. Y., Niu, Y. T., & Piao, J. L. 2019, *PrGeo*, **34**, 1336  
 Wait, J. R. 1959, *PIRE*, **47**, 998  
 Wang, J. 2006, *Chin. J. Radio Sci.*, **21**, 628  
 Wang, Z., Niu, Y. T., Zhou, K. P., et al. 2022, *ChJG*, **65**, 2402  
 Xin, N. 2019, Master's thesis, Xi'an University Of Technology  
 Zhao, X. K., Niu, Y. T., Zheng, Z. Y., et al. 2023, *Ap&SS*, **368**, 10